Theoretical study of flow coupling mechanisms in two-layer Rayleigh-Bénard convection

M. Petry and F. H. Busse
Institute of Physics, University of Bayreuth, D-95440 Bayreuth, Germany
(Received 23 June 2002; revised manuscript received 3 February 2003; published 16 July 2003)

Rayleigh-Bénard convection in a system of two superimposed immiscible fluids, heated from below, is investigated theoretically. In a two-layer system, stationary convection is characterized by two distinct modes of flow coupling, namely, thermal coupling and viscous coupling. We derive two coupled amplitude equations in order to describe the nonlinear interaction of the viscous and the thermal coupling modes, whereby we restrict our analysis to the two-dimensional case. By analyzing the amplitude equations for varying fluid parameters, we make predictions concerning the stability of the involved coupling modes in the weakly nonlinear regime.

DOI: 10.1103/PhysRevE.68.016305 PACS number(s): 47.20.Bp, 47.20.Dr, 47.54.+r

I. INTRODUCTION

The problem of convection in two superimposed horizontal layers of immiscible fluids, heated from below, has attracted much attention in the past decades. Interest in this problem originally arose in the context of thermal convection in the Earth's mantle [1]. Seismic evidence exists for a discontinuity at the depth of 670 km, which is nowadays attributed primarily to a phase change owing to the transition from a spinel to a perovskite crystal lattice of the silicate mantle material. But the contribution of a chemical change at the 670-km seismic discontinuity cannot easily be excluded. Later, work on double-layer convection was motivated by new dynamical phenomena, such as oscillatory convection, which cannot be observed in the case of single-layer convection. The large number of dimensionless parameters that appear in the description of double-layer convection may have discouraged some fluid dynamicists and physicists from entering this area of research. On the other hand, the huge parameter space of the problem offers the opportunity to study a number of dynamical phenomena, such as pattern resonances, in a relatively simple setting that can be realized experimentally. Numerous laboratory realizations of double-layer convection have been performed in the past years and a considerable amount of experimental data have been published. But the agreement between the theoretical predictions and laboratory measurements is not satisfactory in most cases. In part, this is due to the fact that immiscible fluids represent an idealization and that the physical properties of at least one of the pairs of fluids are often not well known. The number of suitable pairs of nearly immiscible fluids is not very large and they span only a limited region in the parameter space. Since, in reality, always some amount of mixing or entrainment happens at the interface between two liquids, the properties of a two-layer convection experiment tend to change in time and there is a limited reproducibility of the results. Moreover, contaminants accumulate at the interface, the properties of which cannot be described solely by the interfacial tension. Interface elasticity and interface viscosity have been introduced [2–6] to describe the deviations of the dynamical properties from that of an uncontaminated interface. We shall return to this point at the end of this paper. The motivation for the weakly nonlinear analysis of this paper comes from the observation that the form of convection often changes at supercritical Rayleigh numbers, which are still sufficiently close to the critical value, such that a weakly nonlinear analysis may be expected to be applicable.

II. BASIC EQUATIONS

We consider two immiscible Newtonian fluids contained in the space between two parallel perfectly heat conducting boundaries of infinite horizontal extension. The lower boundary is kept on a constant temperature T_2 whereas T_1 is the temperature of the upper boundary. We use a set of Cartesian coordinates x,y,z with corresponding unit vectors $\mathbf{i},\mathbf{j},\mathbf{k}$ as indicated in Fig. 1. $\mathbf{k}$ is the unit vector in the vertical direction opposite to the acceleration of gravity $\mathbf{g}=-g\mathbf{k}$. Let d be the thickness, ϱ the density, ν the kinematic viscosity, κ the heat diffusivity, λ the thermal conductivity, and γ the thermal expansion coefficient of the lower fluid. We denote the corresponding properties of the upper fluid with an asterisk. It is reasonable to introduce the following ratios between the properties of the upper and the lower layers:

$$d_0=\frac{d^*}{d},\quad \varrho_0=\frac{\varrho^*}{\varrho},\quad \nu_0=\frac{\nu^*}{\nu},$$

$$\kappa_0=\frac{\kappa^*}{\kappa},\quad \lambda_0=\frac{\lambda^*}{\lambda},\quad \gamma_0=\frac{\gamma^*}{\gamma}.$$

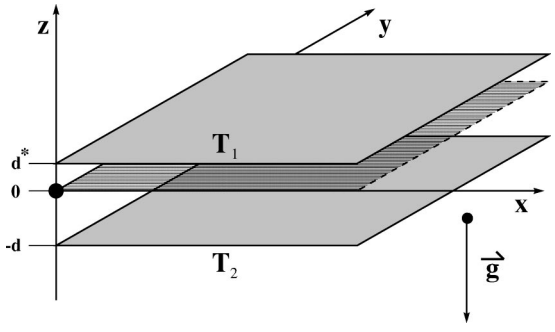

FIG. 1. Geometrical configuration of the two-layer system.

In the basic static state of pure conduction, the interface is flat and located at $z=0$. The temperature at the interface in the basic state is given by

$$T_0=\frac{\lambda^* d T_1+\lambda\, d^* T_2}{\lambda^* d+\lambda d^*}. \tag{1}$$

We describe both layers within the Boussinesq approximation, i.e., all parameters are independent of the temperature, except for the densities and the interface tension. The temperature dependence of the density,

$$\rho=\varrho(1-\gamma(T-T_0)), \tag{2}$$

is taken into account only in the gravity term. Using d as length scale, d^2/κ as time scale, and (T_2-T_0) as scale of the temperature, the basic equations describing the dynamics of the lower fluid, i.e., the Navier-Stokes equation, the equation of heat conduction and the equation of continuity can be written in the following dimensionless form:

$$\frac{1}{P}(\partial_t+\mathbf{v}\cdot\boldsymbol{\nabla})\mathbf{v}=-\boldsymbol{\nabla}\pi+R\theta\mathbf{k}+\boldsymbol{\nabla}^2\mathbf{v}, \tag{3a}$$

$$(\partial_t+\mathbf{v}\cdot\boldsymbol{\nabla})\theta=\mathbf{v}\cdot\mathbf{k}+\boldsymbol{\nabla}^2\theta, \tag{3b}$$

$$\boldsymbol{\nabla}\cdot\mathbf{v}=0, \tag{3c}$$

where $\mathbf{v}$ is the velocity vector, θ and π denote the deviations of the temperature and of the pressure, respectively, from the basic static state. Rayleigh number R and Prandtl number P are defined by

$$R=\frac{\gamma g(T_2-T_0)d^3}{\nu\kappa}, \quad P=\frac{\nu}{\kappa}. \tag{4}$$

Using the same scales, the corresponding equations for the upper fluid read as follows:

$$\frac{1}{P}(\partial_t+\mathbf{v}^*\cdot\boldsymbol{\nabla})\mathbf{v}^*=-\frac{1}{\varrho_0}\boldsymbol{\nabla}\pi^*+\gamma_0 R\theta^*\mathbf{k}+\nu_0\boldsymbol{\nabla}^2\mathbf{v}^*, \tag{5a}$$

$$(\partial_t+\mathbf{v}^*\cdot\boldsymbol{\nabla})\theta^*=\frac{1}{\lambda_0}\mathbf{v}^*\cdot\mathbf{k}+\kappa_0\boldsymbol{\nabla}^2\theta^*, \tag{5b}$$

$$\nabla\cdot\mathbf{v}^*=0. \tag{5c}$$

For simplicity, we assume that the motion occurs in the form of two-dimensional rolls. Therefore, we can introduce two streamfunctions $\psi=\psi(x,z)$ and $\psi^*=\psi^*(x,z)$ in order to express the velocities as follows:

$$\mathbf{v}=\boldsymbol{\nabla}\times\psi\,\mathbf{j}=(-\partial_z\psi,0,\partial_x\psi),$$

$$\mathbf{v}^*=\boldsymbol{\nabla}\times\psi^*\mathbf{j}=(-\partial_z\psi^*,0,\partial_x\psi^*). \tag{6}$$

By taking the curl of Eqs. (3a) and (5a) and multiplying them with $\mathbf{j}$, we obtain the following four equations:

$$\boldsymbol{\nabla}^4\psi+R\partial_x\theta-\frac{1}{P}\partial_t\boldsymbol{\nabla}^2\psi=\frac{1}{P}[\psi,\boldsymbol{\nabla}^2\psi], \tag{7a}$$

$$\partial_x\psi+\boldsymbol{\nabla}^2\theta-\partial_t\theta=[\psi,\theta], \tag{7b}$$

$$\nu_0\boldsymbol{\nabla}^4\psi^*+\gamma_0 R\partial_x\theta^*-\frac{1}{P}\partial_t\boldsymbol{\nabla}^2\psi^*=\frac{1}{P}[\psi^*,\boldsymbol{\nabla}^2\psi^*], \tag{7c}$$

$$\frac{1}{\lambda_0}\partial_x\psi^*+\kappa_0\boldsymbol{\nabla}^2\theta^*-\partial_t\theta^*=[\psi^*,\theta^*], \tag{7d}$$

where $[.,.]$ is the Poisson operator, i.e., $[f_1,f_2]=\partial_x f_1\partial_z f_2-\partial_x f_2\partial_z f_1$. Finally, we rewrite Eqs. (7a)–(7d) for state vector $\mathbf{y}=(\psi,\theta,\psi^*,\theta^*)$ in the form

$$(\mathbf{L}+R\mathbf{M}+\partial_t\mathbf{T})\mathbf{y}=\mathbf{N}(\mathbf{y},\mathbf{y}). \tag{8}$$

The structure of linear operators $\mathbf{L},\mathbf{M},\mathbf{T}$ and of the nonlinear operator $\mathbf{N}$ can easily be obtained from Eqs. (7a)–(7d).

III. BOUNDARY AND INTERFACE CONDITIONS

We use no-slip Eq. (9a) as well as stress-free boundary conditions (9b), together with fixed temperatures at the outer boundaries of the double layer, which are located at $z=-1$ and $z=d_0$:

$$\partial_x\psi=\partial_z\psi=\theta=0 \text{ at } z=-1,$$

$$\partial_x\psi^*=\partial_z\psi^*=\theta^*=0 \text{ at } z=d_0, \tag{9a}$$

$$\partial_x\psi=\partial_z^2\psi=\theta=0 \text{ at } z=-1,$$

$$\partial_x\psi^*=\partial_z^2\psi^*=\theta^*=0 \text{ at } z=d_0. \tag{9b}$$

Distortions of the interface from the equilibrium position are given by $F(x,z,t)=z-\zeta(x,t)=0$. The substantive derivative of F yields the kinematic condition $\partial_t\zeta=\partial_x\psi(\zeta)+\partial_z\psi(\zeta)\partial_x\zeta$ for the material interface. The domain occupied by each fluid is *a priori* unknown and ζ must be determined as part of the solution. While the linear problem with $\zeta\neq0$ can be solved easily [7], the situation becomes rather difficult in the nonlinear case. For many combinations of immiscible fluids, used within laboratory experiments, the interface tension and the density difference between the fluids prevent a significant distortion of the interface. Therefore, we will assume a flat interface between the two liquids. The continuity of the velocity, the temperature, and the heat transport, together with $\zeta=0$, require conditions

$$\partial_x\psi=\partial_x\psi^*$$
$$=\partial_z\psi-\partial_z\psi^*=\theta-\theta^*=\lambda_0\partial_z\theta^*-\partial_z\theta=0 \text{ at } z=0. \tag{10}$$

While the balance of the normal stresses at the interface does not enter the problem in the case $\zeta=0$, the balance of the tangential stresses can be written as

$$\partial_z^2\psi-\nu_0\varrho_0\partial_z^2\psi^*=M\partial_x\theta+N\partial_x^2\partial_z\psi. \tag{11}$$

Marangoni number M and interface viscosity number N are defined by

$$M=-\frac{\partial\sigma}{\partial T}\frac{(T_2-T_0)d}{\eta\kappa},\quad N=\frac{\eta_i}{\eta d}, \tag{12}$$

where η_i is the interface viscosity [3,5,6]. We assume that temperature derivative $\partial\sigma/\partial T$ of interfacial tension σ is constant. Since both the Rayleigh number and the Marangoni number depend on temperature difference (T_2-T_0), typically both parameters are varied simultaneously in experiments. Therefore, we use the dimensionless parameter

$$c:=\frac{M}{R}=-\frac{\partial\sigma}{\partial T}\frac{1}{\varrho_0\gamma g d^2} \tag{13}$$

instead of the Marangoni number. For $|c|\gg 1$ the Marangoni effect will be dominant, while for $|c|\ll 1$ the convection will be driven by buoyancy.

IV. LINEAR ANALYSIS

The linear stability of the double-layer system has been already investigated by numerous authors [7–10]. Nevertheless, we will make some technical remarks concerning the linear problem, since it is equivalent to the first-order problem of the forthcoming nonlinear analysis. The linearized version of Eq. (8)

$$(\mathbf{L}+R_0\mathbf{M}+\partial_t\mathbf{T})\mathbf{y}_0=\mathbf{0} \tag{14}$$

can be solved with ansatz

$$\mathbf{y}_0(x,z,t)=(u(z),\vartheta(z),u^*(z),\vartheta^*(z))e^{i\alpha x+\sigma t}. \tag{15}$$

Therein, α denotes the wave number and $\sigma=\sigma_r-i\omega_0$ is the complex growth rate. In general, the z-depending functions are complex. Since we are interested in the case of marginal stability, i.e., in the neutral curves, we put $\sigma_r=0$. Inserting Eq. (15) into Eq. (14), we find

$$\left(\alpha^2-\frac{i\omega_0}{P}\right)\alpha^2 u+\left(\frac{i\omega_0}{P}-2\alpha^2\right)u''+u''''+i\alpha R_0\vartheta=0, \tag{16a}$$

$$i\alpha u+(i\omega_0-\alpha^2)\vartheta+\vartheta''=0, \tag{16b}$$

$$\left(\nu_0\alpha^2-\frac{i\omega_0}{P}\right)\alpha^2 u^*+\left(\frac{i\omega_0}{P}-\nu_0 2\alpha^2\right)u^{*\prime\prime}+\nu_0 u^{*\prime\prime\prime\prime}+\gamma_0 i\alpha R_0\vartheta^*=0, \tag{16c}$$

$$\frac{1}{\lambda_0}i\alpha u^*+(i\omega_0-\kappa_0\alpha^2)\vartheta^*+\kappa_0\vartheta^{*\prime\prime}=0. \tag{16d}$$

These equations, together with the six boundary conditions of Eq. (9) and the six interface conditions (10) and (11), can be solved by the use of a shooting method, as described in Ref. [7]. The interface conditions provide a set of six linear homogeneous equations whose solvability condition yields an infinite number of neutral curves $R_0^{(n)}(\alpha)$ and dispersion relations $\omega_0^{(n)}(\alpha)$, with $n\in\mathbb{N}$. If we heat from below, every neutral curve is normally characterized by a critical Rayleigh number $R_c^{(n)}=\min_\alpha\{R_0^{(n)}(\alpha)\}=R_0^{(n)}(\alpha_c^{(n)})>0$, a critical wave number $\alpha_c^{(n)}$, and a critical frequency $\omega_c^{(n)}=\omega_0^{(n)}(\alpha_c^{(n)})$. We number the neutral curves consecutively, such that $R_c^{(n)}<R_c^{(n+1)}$ holds for $n\in\mathbb{N}$. In the following, we will restrict our attention to the first two linear unstable modes, which we will denote as the A and B modes, respectively. Of special interest are the critical values $(R_c^{(1)},\alpha_c^{(1)},\omega_c^{(1)})$ of the A mode, of course, since they describe the onset of convection. In the theory of Rayleigh-Bénard convection, the neutral curves for $n>1$ are typically of minor interest because the amplitude of convection becomes quite high for $R\geqslant R_c^{(2)}$. This is true, e.g., for a single layer with stress-free boundaries, where $R_0^{(n)}(\alpha)=(\alpha^2+n^2\pi^2)^3/\alpha^2$ holds and where $R_c^{(2)}=16\times R_c^{(1)}$. In contrast to single-layer convection, the neutral curves $R_0^{(1)}(\alpha)$ and $R_0^{(2)}(\alpha)$ of double-layer convection usually correspond to different types of coupling and $R_0^{(2)}-R_0^{(1)}$ can become relatively small, depending on the system parameters [11]. Therefore, the interaction between the A and B modes may become important for the convection in the weakly nonlinear regime. In particular, this interaction can lead to a change of the coupling mechanism, which is connected with a characteristic change of the flow pattern. Our basic idea is to describe the competition between the A and B modes with the help of two coupled amplitude equations, which we will derive in the following section. For these purposes, we introduce the following notation:

$$\alpha_c:=\alpha_c^{(1)},\quad R_c:=R_0^a:=R_0^{(1)}(\alpha_c),\quad R_0^b:=R_0^{(2)}(\alpha_c). \tag{17}$$

Please note that, in general, $R_0^b\neq R_c^{(2)}$ holds.

V. NONLINEAR ANALYSIS

We perform a weakly nonlinear analysis in the neighborhood of the onset of convection (α_c,R_c). For simplicity, we shall restrict the analysis to the case of a monotonous onset of A and B modes, i.e., we assume $\omega_c^{(1)}=\omega_c^{(2)}=0$. In defining a scalar product

$$\begin{aligned}\langle\mathbf{y}_1,\mathbf{y}_2\rangle:=&\frac{\alpha}{\pi}\int_{-1}^{0}\int_0^{2\pi/\alpha}\overline{\psi_1}\psi_2 dxdz\\&+\frac{\alpha}{\pi}\int_0^{d_0}\int_0^{2\pi/\alpha}\overline{\psi_1^*}\psi_2^* dxdz\\&+\frac{\alpha}{\pi}\int_{-1}^{0}\int_0^{2\pi/\alpha}\overline{\theta_1}\theta_2 dxdz\\&+\frac{\alpha}{\pi}\int_0^{d_0}\int_0^{2\pi/\alpha}\overline{\theta_1^*\theta_2^*} dxdz,\end{aligned} \tag{18}$$

we indicate the complex conjugate by a bar. Let $(\mathbf{L}+R_0\mathbf{M})^\dagger$ be the adjoint operator to $(\mathbf{L}+R_0\mathbf{M})$ and let $\mathbf{y}_0^\dagger$ be a solution of

$$(\mathbf{L}+R_0\mathbf{M})^\dagger\mathbf{y}_0^\dagger=\mathbf{0} \tag{19}$$

Then, amplitude ϵ of convection can be defined by

$$\epsilon := \langle \mathbf{y}_0^\dagger, \mathbf{y} \rangle \tag{20}$$

and the expansion in powers of ϵ can be written in the form

$$R = R_0 + \epsilon R_1 + \epsilon^2 R_2 + \cdots, \tag{21a}$$

$$\mathbf{y} = \epsilon(\mathbf{y}_0 + \epsilon \mathbf{y}_1 + \epsilon^2 \mathbf{y}_2 + \cdots). \tag{21b}$$

For time-dependent processes we shall introduce a slow time $T := \epsilon^2 t$ such that ∂_t is replaced by $\epsilon^2 \partial_T$. Since we fix the Marangoni number by $M = cR$, there is no need to write a separate expansion for M. By inserting expansion (21b) into definition (20) we obtain the set of conditions

$$\langle \mathbf{y}_0^\dagger, \mathbf{y}_n \rangle = \delta_{0n}, \quad n = 0,1, \ldots . \tag{22}$$

Insertion of expressions (21a) and (21b) into Eq. (8) yields the linear Eq. (14) in lowest order. We write the solutions for the A and B modes in the form

$$\mathbf{y}_0^a(x,z) = \frac{1}{2} A_0(T)([u_a(z), \vartheta_a(z), u_a^*(z), \vartheta_a^*(z)] e^{i\alpha x} + \text{c.c.}), \tag{23a}$$

$$\mathbf{y}_0^b(x,z) = \frac{1}{2} B_0(T)([u_b(z), \vartheta_b(z), u_b^*(z), \vartheta_b^*(z)] e^{i\alpha x} + \text{c.c.}), \tag{23b}$$

where c.c. indicates the complex conjugate of the first term in the respective brackets. We have introduced complex amplitudes A_0 and B_0 which may depend on slow time T in addition to their dependence on the external parameters of the problem such as R. Wave number α will usually be fixed at its critical value $\alpha = \alpha_c$. Sum

$$\mathbf{y}_0 = \mathbf{y}_0^a + \mathbf{y}_0^b \tag{24}$$

of the two modes is the starting point of the following weakly nonlinear analysis. Of course, since Rayleigh numbers R_0^a and R_0^b, for which $\mathbf{y}_0^a$ and $\mathbf{y}_0^b$ solve the linear equations, are not equal in general, $\mathbf{y}_0$ solves the linear problem only approximately, to the extent that the difference $R_0^b - R_0^a$ is small such that it can be taken into account in the higher order of the problem. Since the conditions (22) do not fix the amplitude of $\mathbf{y}_0$, we use the normalization

$$\int_{-1}^{0} |u_a|^2 dz + \int_0^{d_0} |u_a^*|^2 dz = \int_{-1}^{0} |u_b|^2 dz + \int_0^{d_0} |u_b^*|^2 dz = 1. \tag{25}$$

In order ϵ^2 of Eq. (8), we obtain the linear inhomogeneous equation

$$(\mathbf{L} + R_0 \mathbf{M}) \mathbf{y}_1 = -R_1 \mathbf{M} \mathbf{y}_0 + \mathbf{N}(\mathbf{y}_0, \mathbf{y}_0) \tag{26}$$

which requires the solvability condition

$$R_1 = \frac{\langle \mathbf{y}_0^\dagger, \mathbf{N}(\mathbf{y}_0, \mathbf{y}_0) \rangle}{\langle \mathbf{y}_0^\dagger, \mathbf{M} \mathbf{y}_0 \rangle} \tag{27}$$

since its homogeneous part has a nonvanishing solution. It can readily be checked that condition (27) is satisfied with $R_1 = 0$ and solution $\mathbf{y}_1$ of Eq. (26) can thus be written in the form

$$\psi_1(x,z) = \frac{1}{2}([A_0^2 u_{a1}(z) + A_0 B_0 u_{ab1}(z) + B_0^2 u_{b1}(z)] e^{i2\alpha x} + |A_0|^2 u_{a2}(z) + A_0 \overline{B}_0 u_{ab2}(z) + |B_0|^2 u_{b2}(z) + \text{c.c.}), \tag{28}$$

$$\theta_1(x,z) = \frac{1}{2}([A_0^2 \vartheta_{a1}(z) + A_0 B_0 \vartheta_{ab1}(z) + B_0^2 \vartheta_{b1}(z)] e^{i2\alpha x} + |A_0|^2 \vartheta_{a2}(z) + A_0 \overline{B}_0 \vartheta_{ab2}(z) + |B_0|^2 \vartheta_{b2}(z) + \text{c.c.}), \tag{29}$$

with analogous expressions valid in the upper layer which differs only by an asterisk at the z-depending functions. It is evident that the orthogonality condition (22) is satisfied. For the determination of the functions $u_{a1}(z), u_{a1}^*(z), u_{ab1}(z), \ldots$ the shooting method has been employed and value

$$R_0 := \frac{1}{2}(R_0^a + R_0^b) \tag{30}$$

has been used. Because of the closeness of R_0^a and R_0^b, the results are changed only negligibly if, for instance, $R_0 = R_0^a$ is assumed. It can easily be demonstrated that functions $u_{a2}, u_{a2}^*, u_{b2}, u_{b2}^*$ vanish identically but the same does not hold for u_{ab2} and u_{ab2}^*. In order ϵ^3, we obtain equation

$$(\mathbf{L} + R_0 \mathbf{M}) \mathbf{y}_2 = \partial_T \mathbf{T} \mathbf{y}_0 - R_2 \mathbf{M} \mathbf{y}_0 + \mathbf{N}(\mathbf{y}_0, \mathbf{y}_1) + \mathbf{N}(\mathbf{y}_1, \mathbf{y}_0) \tag{31}$$

which requires the solvability condition

$$R_2 \langle \mathbf{y}_0^\dagger, \mathbf{M} \mathbf{y}_0 \rangle = \langle \mathbf{y}_0^\dagger, \partial_T \mathbf{T} \mathbf{y}_0 \rangle + \langle \mathbf{y}_0^\dagger, \mathbf{N}(\mathbf{y}_0, \mathbf{y}_1) \rangle + \langle \mathbf{y}_0^\dagger, \mathbf{N}(\mathbf{y}_1, \mathbf{y}_0) \rangle. \tag{32}$$

Since $\mathbf{y}_0^{a\dagger}$ as well as $\mathbf{y}_0^{b\dagger}$ can be used in place of $\mathbf{y}_0^\dagger$, two coupled nonlinear amplitude equations are obtained. By diagonalizing the contributions from the T-operator term, the two equations can be written as differential equations $\partial A_0 / \partial T = \ldots$ and $\partial B_0 / \partial T = \ldots$. In order to gain a direct connection with the original Eqs. (8), we now eliminate ϵ by writing

$$A := \epsilon A_0, \quad B := \epsilon B_0, \quad R_2 = \frac{R - R_0}{\epsilon^2}, \quad \epsilon^2 \frac{\partial}{\partial T} = \frac{\partial}{\partial t}$$

whereby, we neglect contributions of higher order in ϵ. We thus obtain the final form of the amplitude equations

$$\partial_t A = (a_1 r_a + a_2 r_b) A + (a_3 r_a + a_4 r_b) B + a_5 A|A|^2 + a_6 B|A|^2 + a_7 B^2 \overline{A} + a_8 A^2 \overline{B} + a_9 A|B|^2 + a_{10} B|B|^2, \tag{33a}$$

$$\partial_t B = (b_1 r_a + b_2 r_b)A + (b_3 r_a + b_4 r_b)B + b_5 A|A|^2 + b_6 B|A|^2 + b_7 B^2 \overline{A} + b_8 A^2 \overline{B} + b_9 A|B|^2 + b_{10} B|B|^2, \quad (33b)$$

where definitions $r_a := (R - R_0^a)$ and $r_b := (R - R_0^b)$ have been used. All coefficients in Eqs. (33) are real.

VI. RESULTS

Since it is not feasible to investigate the entire parameter space with the system of amplitude Eqs. (33), we shall restrict the attention to a few typical special cases including the case of an experiment [7]. In the following examples $M = N = 0$ is assumed. Since a supercritical bifurcation of the A mode at $R = R_c$ was always found, the properties of the A mode will persist for a certain interval $R - R_c > 0$. We are interested in the case when the interaction between the two fluid layers changes discontinuously through the nonlinear coupling with the B mode. In the following, we analyze such a situation for stress-free as well as for rigid boundaries. When the Rayleigh numbers in the two layers are approximately equal ($R \approx R^*$), buoyancy-driven convection will occur in both the layers for $R > R_c$. In this case we can distinguish between viscous (mechanical) coupling and thermal coupling. Viscous coupling is characterized by an opposite sense of circulation in the layers. Accordingly, the tangential velocity on both sides of the interface has the same sign and the stronger circulation may support the weaker one on the other side. In the special case when no stress is exerted from one layer onto the other, stress-free conditions are obtained. Because of the opposite sense of circulation, the temperature perturbation also has the opposite sign in both the layers in the case of viscous coupling. In the case of thermal coupling the temperature perturbation has the same sign and it is thus less constrained. The corresponding buoyancy force drives convection with the same sense of circulation in both the layers. When the viscosities of the two layers are of the same order, viscous coupling is preferred at the onset of convection. Otherwise, the effects of heat conduction lead to thermal coupling. It is possible for the system to oscillate between viscous and thermal coupling. This type of time-dependent convection is called oscillatory coupling [7].

A. Case 1: $d_0 = \kappa_0 = \lambda_0 = \varrho_0 = \eta_0 = \gamma_0 = 1$

In this case the material properties of both the layers are the same and the linear analysis can be carried out easily [7]. The neutral curves for viscous and thermal coupling are shown in Fig. 2 for rigid as well as for stress-free boundaries. The corresponding functions $u(z), \vartheta(z)$ for stress-free boundaries are displayed in Fig. 3. Since all quantities plotted are dimensionless, no units are needed. This is true for all figures in this article. Both the A as well as the B mode satisfy the six boundary conditions (9a) and (9b), respectively, and the six interface conditions (10) and (11). The A mode exhibits antisymmetric functions $u(z), \vartheta(z)$ with respect to $z = 0$, while these functions are symmetric for the B mode. This clear distinction by symmetry (and orthogonality) between A and B modes disappears as one moves away from point $d_0 = \kappa_0 = \lambda_0 = \varrho_0 = \eta_0 = \gamma_0 = 1$ in the parameter space. But A and B modes still resemble the ideal case of Fig. 3 as long as the properties of the two layers do not become too different. The A mode is an example for pure viscous coupling since we find $u'' = u^{*\prime\prime} = 0$ and $\vartheta = \vartheta^* = 0$ for the A mode at $z = 0$, so that the interface becomes a stress-free isotherm. This result is independent of wave number α and therefore, the neutral curve $R_0^a(\alpha)$ for the A mode in the case of rigid boundaries corresponds to the neutral curve in a Rayleigh-Bénard layer with one rigid and one stress-free boundary. We thus have $R_c = R_0^a = 1101$ with $\alpha_c = 2.682$. This result is well known (Pellew and Southwell, Ref. [12]) and has been confirmed by Rasenat, Busse, and Rehberg [7]. The B mode is an example for pure thermal coupling since $u' = u^{*\prime} = 0$ and $\vartheta' = \vartheta^{*\prime} = 0$ holds at $z = 0$, so that the interface becomes rigid (vanishing velocity) and thermally insulating. Therefore, the neutral curve for the B mode in the case of rigid boundaries corresponds to the neutral curve of a Rayleigh-Bénard layer with a rigid and thermally insulating boundary on one side and a rigid, isothermal boundary on the other side. We find $R_0^b = 1299$ in this case for $\alpha = 2.682$. Similarly, the neutral curve for stress-free boundaries can be obtained readily; $R_c = R_0^a = 27\pi^4/4 = 657.5$ with $\alpha_c = \pi/\sqrt{2}$ for the A mode and $R_0^b = 816.7$ for the B mode. The bifurcation diagram obtained from ampli-

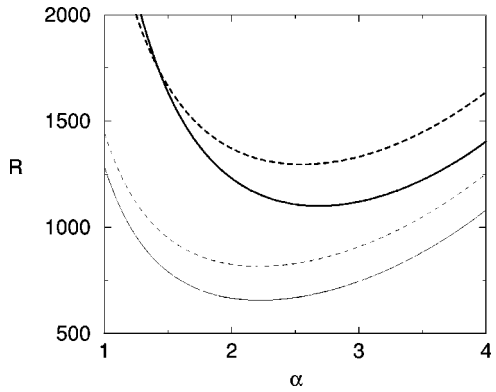

FIG. 2. Neutral curves for viscous (solid lines) and thermal (dashed lines) coupling in case $d_0 = \kappa_0 = \lambda_0 = \varrho_0 = \eta_0 = \gamma_0 = 1$. Thick (thin) lines correspond to rigid (stress-free) boundaries.

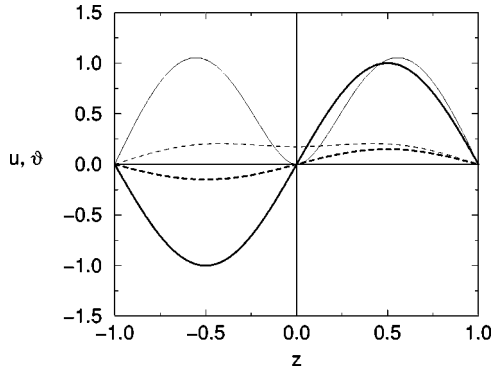

FIG. 3. Functions $u(z)$ (solid) and $\vartheta(z)$ (dashed) for the A (thick) and B modes (thin) in case $d_0 = \kappa_0 = \lambda_0 = \varrho_0 = \eta_0 = \gamma_0 = 1$, with stress-free boundaries corresponding to $\alpha_c = 2.221, R_0^a = 657.5, R_0^b = 816.7$.

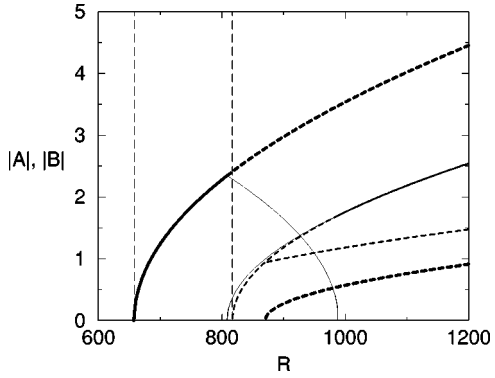

FIG. 4. Bifurcations in the case of stress-free boundary conditions. Diagram for $d_0=\kappa_0=\lambda_0=\varrho_0=\eta_0=\gamma_0=1$.

tude Eqs. (33a) and (33b) in the case of stress-free boundaries with $P=1$ is shown in Fig. 4. In our bifurcation diagrams, thick lines correspond to $|A|$, thin lines correspond to traveling waves, and lines of medium thickness correspond to $|B|$. Solid lines indicate stable solutions while dashed lines indicate unstable solutions. A single branch of states containing both A and B components is represented by two curves, one for each component. At $R=808.2$ a bifurcation occurs in which a traveling wave branch (two thin lines, one for $|A|$ and one for $|B|$) emerges from the A mode. The latter becomes unstable while the property of stability is taken over by the traveling waves. The frequency of the traveling waves increases from zero at the bifurcation point and decreases back to zero as the traveling wave solution meets the B mode in a second bifurcation at $R=988.7$. While the two layers convect with viscous coupling at low supercritical Rayleigh numbers, the traveling waves provide a transition from viscous to thermal coupling, represented by the stable B mode for $R>988.7$. In addition, there is a mixed mode solution which bifurcates at $R=R_m=869.6$ from the B mode. The heat transport carried by the various types of convection is plotted in Fig. 5, which demonstrates that the solution with the maximum Nusselt number is not always the stable solution.

When no-slip, instead of stress-free, boundaries are used, the forms of the A and the B modes are changed very little,

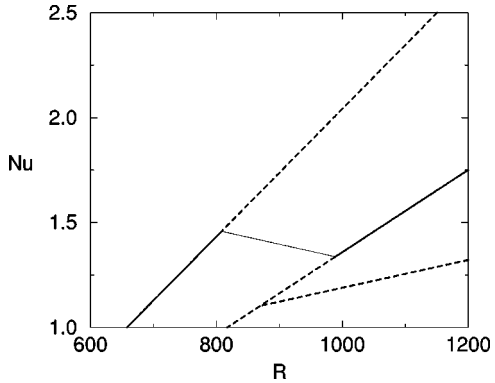

FIG. 5. Nusselt numbers as function of the Rayleigh number for the bifurcating solutions in case $P=d_0=\kappa_0=\lambda_0=\varrho_0=\eta_0=\gamma_0=1$ with stress-free boundary conditions.

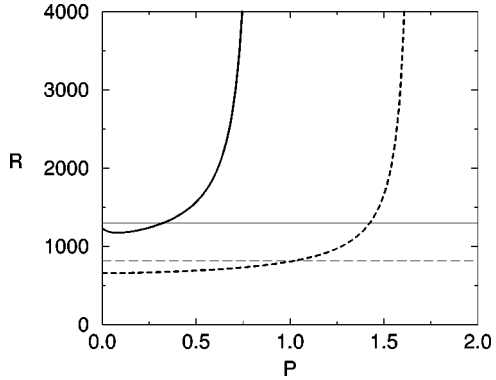

FIG. 6. The Rayleigh number at which the A mode becomes unstable as function of the Prandtl number for $d_0=\kappa_0=\lambda_0=\varrho_0=\eta_0=\gamma_0=1$ with rigid (solid line) or stress-free (dashed line) boundaries. The thin lines indicate the corresponding value of R_0^b.

except for $u(z)$ close to the boundaries. However, the transition from viscous to thermal coupling no longer occurs for $P=1$. Since the Prandtl number enters only the nonlinear part of the problem and since it measures the ratio between the strength of viscous and thermal diffusion, a lowering of the Prandtl number is likely to promote thermal coupling. This expectation is indeed fulfilled, as shown in Fig. 6. Rayleigh number R_i^a, at which the A mode becomes unstable has been plotted here as a function of the Prandtl number. There exists an upper limit of P for which a finite value of R_i^a can be obtained. This upper limit P_i^a assumes value $P_i^a=1.660$ for stress-free boundaries while for no-slip boundaries, $P_i^a=0.823$ is found. From the value of R_0^b, also shown in the figure, one can infer that for $P=0.3$ approximately the same bifurcation diagram as Fig. 4 can be obtained for rigid boundaries, as was obtained for stress-free boundaries in case $P=1$.

B. Case 2: $d_0=\varrho_0=\gamma_0=1$, $\eta_0=25$, $\kappa_0=\lambda_0=0.2$

We now consider a case characterized by thermal coupling at the onset of convection. The neutral curves for the A as well as the B mode are identical with those in case 1. This is true for rigid as well as for stress-free boundaries. Accordingly, the Rayleigh numbers in both layers are equal, i.e., $R=R^*$, and the values of α_c, R_0^a, and R_0^b are the same as in case 1. This property is not quite obvious and is stated here as an empirical fact. It will be the subject of a proof given in a future paper. We first analyze the case of rigid boundaries. Since the upper layer has a much higher viscosity and a lower heat conductivity than the lower layer, the velocity field is much stronger in the lower layer while the temperature perturbation is amplified in the upper layer, as can be seen from Fig. 7. Both A and B modes represent thermal coupling since viscous coupling is minimized owing to the high viscosity ratio $\eta_0=25$. In fact, the lower boundary of the upper layer acts essentially like a stress-free interface, while the high temperature gradient caused in the upper layer by the small value 0.2 of κ_0 and λ_0 exerts a strong influence on the lower layer. The latter effect would disappear for $\kappa_0=\lambda_0=1$ in which case $R^*\ll R$ is obtained with viscous cou-

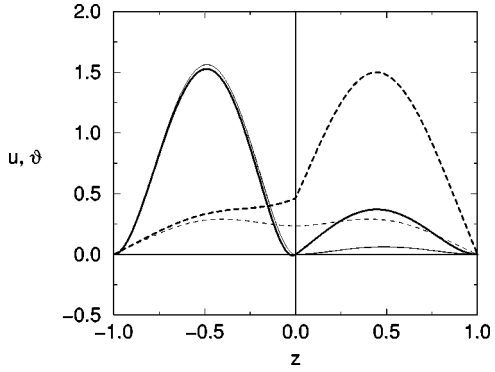

FIG. 7. Functions $u(z)$ (solid) and $\vartheta(z)$ (dashed) for the A (thick) and B (thin) modes in case $P=d_0=\varrho_0=\gamma_0=1, \eta_0=25$, $\kappa_0=\lambda_0=0.2$ with no-slip boundaries corresponding to $\alpha_c=2.682$, $R_0^a=1101$, and $R_0^b=1299$.

pling as a consequence. Similarly, $\eta_0=1$ with $\kappa_0=\lambda_0=0.2$ would lead to $R^* \gg R$ with viscous coupling at the onset of convection. The A solution, bifurcating at the onset of convection, is of mixed type, with the amplitude of the A mode always far exceeding that of the B mode, i.e., $|A| \gg |B| > 0$. Therefore we have multiplied the amplitude of the B mode by factor 10 in Fig. 8. While the A solution is always stable the B solution bifurcating at $R=R_0^b$ is always unstable, which is understandable on the basis of its much lower Nusselt number, as shown in Fig. 9. These properties are not affected by the onset, at $R=R_m=1455$, of two other solutions of mixed type through a saddle node bifurcation. Since these solutions are also unstable they are not of physical interest. Because of the weak mechanical coupling no significant changes can be expected for increasing Rayleigh number within the realm of the amplitude equation description. This property persists when the rigid boundaries are replaced by stress-free boundaries. The effect of the thermal coupling is so strong that a change of the conditions at the outer boundaries will not affect the dynamics of the system in any qualitative way.

C. Case 3: Ethylene glycol-oil system, no-slip boundaries

We now consider an experiment performed by Rasenat, Busse, and Rehberg [7]. Two channels with dimensions 90

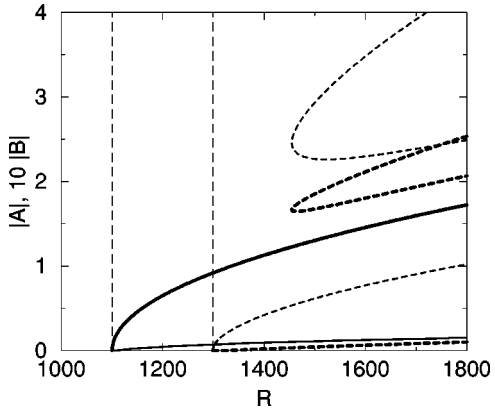

FIG. 8. Bifurcations in the case of no-slip boundary conditions. Diagram for $P=d_0=\varrho_0=\gamma_0=1$, $\eta_0=25$, and $\kappa_0=\lambda_0=0.2$.

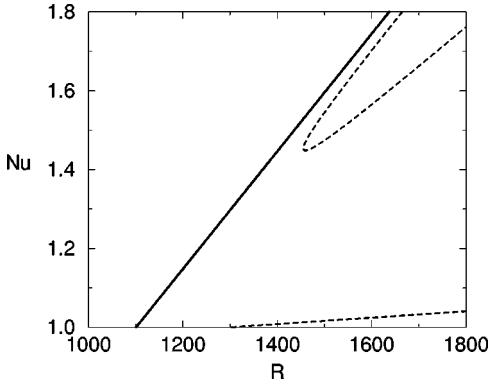

FIG. 9. Nusselt numbers as function of the Rayleigh number for the bifurcating solutions in case $P=d_0=\varrho_0=\gamma_0=1$, $\eta_0=25$, and $\kappa_0=\lambda_0=0.2$ with no-slip boundary conditions.

$\times 20 \times 12$ mm^3 and $140 \times 8 \times 12$ mm^3 have been used with copper plates as boundaries at top and bottom and glass plates as vertical boundaries. Convection rolls tend to orient themselves with the axis perpendicular to the long side of the channel. In the case of the 20-mm wide channel the critical Rayleigh number for onset of convection does not differ much from the value for an infinitely extended layer, but in the case of the 8-mm wide channel the critical Rayleigh number is increased significantly. Among the various combinations of liquids used by Rasenat, Busse, and Rehberg [7] we shall consider here only the system ethylene glycol oil. According to the data given in Ref. [7] we find the following values for the parameters of our theory (ethylene glycol represents the lower fluid layer):

$$P=187, \quad P^*=286, \quad \frac{R^*}{R}=1.886, \quad d_0=1.0,$$

$$\kappa_0=0.966,$$

$$\lambda_0=0.6, \quad \varrho_0=0.811, \quad \eta_0=1.196, \quad \nu_0=1.475,$$

$$\gamma_0=1.613.$$

No data are available for the interfacial tension and its temperature dependence. For simplicity we start with assumption $c=0$. Because of $R^*=1.886R$ convection is first seen in the upper layer. The neutral curves for A and B modes are shown in Fig. 10. According to Fig. 11 the A mode (B mode) corresponds more or less to viscous (thermal) coupling. Critical wave number is $\alpha_c=2.673$, corresponding to $R_0^a=632.9$, while $R_0^b=1199$. These values correspond to $\Delta T_c=2.207$ K and $\Delta T_0^b=4.181$ K in the experimental configuration. The former value is in good agreement with observed onset of convection in the upper layer at $\Delta T_c=2.1\pm0.2$ K in the wider channel. Convection can first be observed in the lower layer at $\Delta T=2.7\pm0.2$ K at which point thermal coupling is found. In the narrow channel a transition from viscous coupling (at $\Delta T=4.1$ K) to thermal coupling (for $\Delta T \geqslant 5.3$ K) could actually be observed, connected with a change to a larger wavelength (from 13.2 mm to 14.5 mm). The latter value agrees quite well with minimum wave number $\alpha_c^b=2.577$ (corresponding to $\lambda_c^b=14.6$ mm) of the neutral curve for the B mode. Since an increase of the wave-

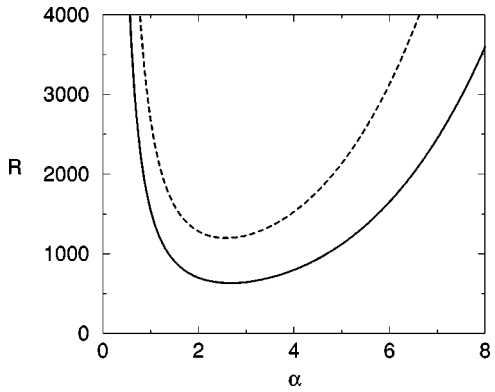

FIG. 10. Neutral curves for the ethylene glycol-oil system with rigid boundaries. The solid (dashed) line corresponds to viscous (thermal) coupling.

length was also observed in the wide cell at $\Delta T \approx 3$ K, the authors of Ref. [7] conclude that the transition from viscous to thermal coupling occurs in this case as well, even though convection in the lower layer was too weak to be observed for $\Delta T < 2.7$ K.

In contrast to the linear aspects of the theory, not even qualitative agreement between predictions and observations, with respect to nonlinear properties, could be found. The bifurcation diagram, based on the amplitude Eqs. (33) and shown in Fig. 12, indicates that only the *A* mode corresponding to viscous coupling is stable. A transition from viscous to thermal coupling is more likely at lower Prandtl numbers. But in the present case with $c=0$, this transition occurs only for $P < P_i^a = 0.624$. Another attempt to resolve the discrepancy through consideration of cases $c \neq 0$ has also not been successful either. Clearly, the Marangoni number does not vanish in the experiment as assumed so far. As c increases from zero the neutral curves of *A* and *B* modes approach each other, as shown in Fig. 13, such that at $c=0.130$ convection sets in with oscillatory coupling (OC). This property is due to the fact that the interfacial tension and motion at the interface have the same direction in the case of the *B* mode, but are opposite for the *A* mode. In the case of negative c the distance between the neutral curves of *A* and *B* modes increases while the distance between the neutral curves of *B* and *C* modes (third linearly unstable mode) decreases until at $c=-0.517$ a new mode with oscillatory coupling replaces the *B* mode as second linearly unstable mode. The nonlinear analysis based on Eqs. (33) has been carried out for different values of $c \in [-0.517, 0.130]$, but the bifurcation diagrams do not show any significantly better agreement with the experimental findings, than for case $c=0$.

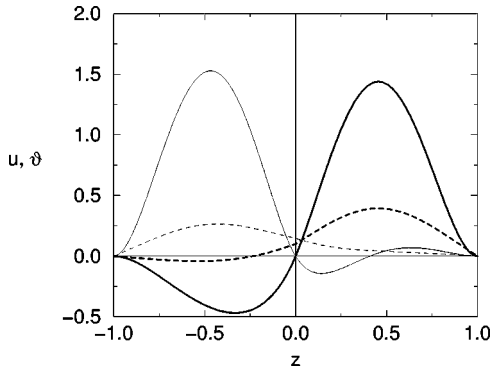

FIG. 11. Functions $u(z)$ (solid) and $\vartheta(z)$ (dashed) of the *A* (thick) and *B* (thin) modes for the ethylene glycol-oil double layer with rigid boundaries corresponding to $\alpha_c = 2.673$, $R_0^a = 632.9$, and $R_0^b = 1199$.

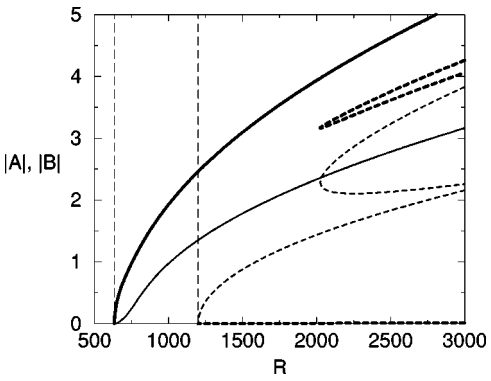

FIG. 12. Bifurcation diagram for the ethylene glycol-oil double layer with rigid boundaries.

Even when depth ratio d_0 was decreased to $d_0 = 0.853$ in order to achieve a state with $R = R^*$, which is expected to favor thermal coupling, no significant change with respect to case $d_0 = 1$ was obtained. It is unlikely that the finite aspect ratios of the experimental configurations are responsible for the discrepancy, especially since the linear theory agrees quite well with the observations of convection in the wider channel. The additional viscous dissipation induced by the sidewall is likely to increase rather than decrease the effective Prandtl number. We are thus led to consider other physical effects not usually taken into account in theoretical treatments of the double-layer convection problem. The foremost candidate for such an effect is impurities on the interface, which are known to exert a strong influence on the dynamical properties of the interface [3,5,6].

In order to study the influence of the interface viscosity number *N*, bifurcation diagrams have been calculated for different values of *N*. As *N* is increased from zero, the *A* mode changes its coupling property continuously from viscous

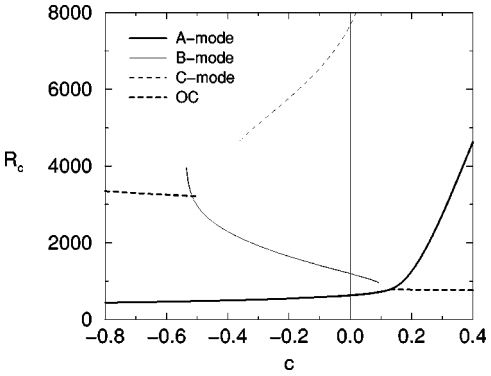

FIG. 13. R_c of the first three linearly unstable modes as function of parameter c for the ethylene glycol-oil double layer with rigid boundary conditions.

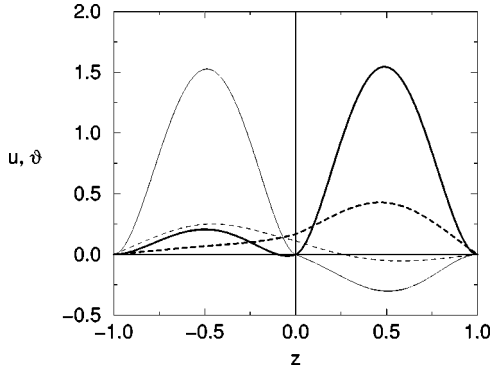

FIG. 14. The functions $u(z)$ (solid) and $\vartheta(z)$ (dashed) of the A (thick) and B (thin) modes for the ethylene glycol-oil double layer with $N=10$ and rigid boundaries corresponding to $\alpha_c=2.746$, $R_0^a=778.5$, and $R_0^b=1427$.

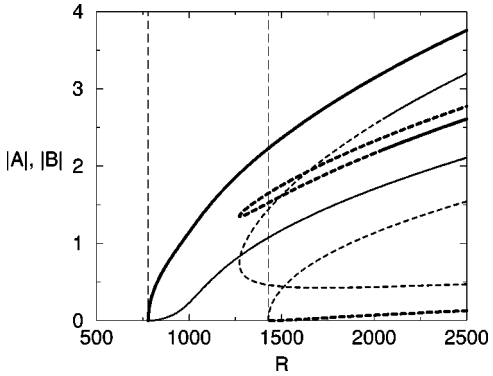

FIG. 15. Bifurcation diagram for the ethylene glycol-oil double layer with $N=10$ and rigid boundaries.

coupling towards thermal coupling. The B mode exhibits the opposite behavior in that it changes from thermal to viscous coupling. Already at $N=2$ temperature function $\vartheta(z)$ of the A mode no longer changes sign throughout the double layer $-1<z<1$, as is characteristic for thermal coupling, although the velocity field still retains some resemblance with viscous coupling through the opposite sense of circulation on both side of the interface. At $N=5$ this feature has also disappeared and the A mode is thermally coupled entirely, while the B mode is completely viscously coupled. The mixed A solution which for $N=2$ still represents the only stable solution, becomes unstable beyond $R>2.72R_0^a$ when N is increased to 5. In Fig. 14 functions $u(z)$ and $\vartheta(z)$ are shown for A and B modes for case $N=10$. At this point $R_0^a=778.5$ and $R_0^b=1427$ are found, corresponding to $\alpha_c=2.746$. As is evident from the bifurcation diagram shown in Fig. 15, the A mode now again is the only stable mode. This property does not change with a further increase of N, not even in the limit case $N=\infty$, which corresponds to condition $\vec{v}=\vec{0}$ at the interface and which, thus, can be investigated easily.

The results obtained for finite values of N are in qualitative agreement with the observations of Rasenat, Busse, and Rehberg [7] except at small N and for an interval around $N=5$. We thus conclude that a transition from viscous to thermal coupling did not occur in the wide channel experiment of Rasenat, Busse, and Rehberg [7]. Instead, it appears to be most likely that convection in the two layers was thermally coupled already at onset, as is suggested by the effects of an interface viscosity and by the absence of any noticeable motion in the lower layer for $\Delta T<2.7$ K. The concept of the interface viscosity may not be the most physically realistic one. But other more realistic descriptions of the effects of impurities are likely to lead to similar results.

VII. CONCLUDING REMARKS

Double-layer convection offers a large variety of scenarios for the nonlinear dynamics of coupled systems, which have only partly been explored in this paper. A major difficulty for the quantitative comparisons between theoretical predictions and experimental measurements is the role played by processes at the interface between the fluids. A detailed exploration of the dynamical effects of impurities at the interface is desirable. The quantitative measurements of the changes induced by the intentional introduction of impurities at the interface could be helpful in this respect. The analysis of this paper has been focused on the case where convection rolls assume the same wavelength in both layers. But interesting interaction can also be expected when the heights of the layers differ significantly such that wavelength ratios of 1:2 or others can be expected. The 1:2 resonance has been considered by Proctor and Jones [13] and experimental realizations of such a system will be of much interest. Similarly, the exploration of the nonlinear properties of oscillatory types of double-layer convection deserves more attention than could be given in the present paper.

[1] F.M. Richter and C.E. Johnson, J. Geophys. Res. **79**, 1635 (1974).
[2] Ph. Cardin and H.-C. Nataf, Europhys. Lett. **14**, 655 (1991).
[3] Ph. Cardin, H.-C. Nataf, and Ph. Dewost, J. Phys. II **1**, 599 (1991).
[4] H.-C. Nataf, S. Moreno, and Ph. Cardin, J. Phys. (France) **49**, 1707 (1988).
[5] L.E. Scriven and C.V. Sternling, J. Fluid Mech. **19**, 321 (1964).
[6] S. Wahal and A. Bose, Phys. Fluids **31**, 3502 (1988).
[7] S. Rasenat, F.H. Busse, and I. Rehberg, J. Fluid Mech. **199**, 519 (1989).
[8] Y. Renardy and D.D. Joseph, Phys. Fluids **28**, 788 (1985).
[9] R.W. Zeren and W.C. Reynolds, J. Fluid Mech. **53**, 305 (1972).
[10] G.Z. Gershuni and E.M. Zhukhovitskii, Sov. Phys. Dokl. **27**, 531 (1982).
[11] A. Prakash, K. Yasuda, F. Otsubo, K. Kuwahara, and T. Doi, Exp. Fluids **23**, 252 (1997).
[12] A. Pellew and R.V. Southwell, Proc. R. Soc. London, Ser. A **176**, 312 (1940).
[13] M.R.E. Proctor and C.A. Jones, J. Fluid Mech. **188**, 301 (1988).